Supplementary methods

Plasmid construction details:

All plasmids were cloned using *E. coli* strain DH5α and regular cloning methods. In general, plasmids were designed for integration of appropriate DNA fragments into the *B. subtilis* chromosome by DOUBLE crossover. The following list provides a brief description of the plasmid constructed. Strains, full sequences and detailed construction methods are available upon request from A.E. Below, all plasmids replicate in *E. coli* but not in *B. subtilis*; details of integration position, selection marker and integration cassette are given in parenthesis:

i. **pVK317** (*ppsB*::P_{spoIIQ}-*spoIIR Neo*^{R}) **–** We first constructed a *ppsB* integration vector containing a *Neo*^{R} gene and two fragments of the *ppsB* gene (515bp fragment starting at position 4066 of the *ppsB* nucleotide sequence and 1190bp starting at position 4864). We inserted into this vector a fragment starting 500 bp upstream of the *spoIIQ* gene and ending at the natural PvuII site occurring 110bp into the *spoIIQ* gene. This fragment was followed by another containing the *spoIIR* RBS and gene, starting 25bp before the *spoIIR* start codon and ending 38bp after the stop codon.

ii. **pVK325** (*ppsB*::P_{spoIIR}-*spoIIR Neo*^{R}) – The pVK317 *spoIIQ* upstream fragment and the *spoIIR* fragment described above were replaced by a single *spoIIR* fragment starting 964bp upstream of the *spoIIR* start codon and ending 38bp downstream of it.

iii. **AEC326** (*ppsB*::P_{spoIIQ}-*spoIIR* Erm) – The *Neo*^{R} resistance gene of pVK317 was replaced by the *Erm*^{R} resistance gene from ECE119 (obtained from BGSC) by cloning into the BsrGI sites of pVK317.

iv. **AEC127** (*sacA*:: *yfp Cm*^{R}) – We used ECE174 (*sacA* integration plasmid[1]) from the BGSC to construct a YFP reporter plasmid, where a codon-optimized version of Venus with a strong ribosome binding site, and two terminators were inserted between the EcoRI and BamHI sites of ECE174, eliminating these sites. A new multiple cloning site with EcoRI and BamHI sites was formed before the RBS to enable the introduction of reporter promoter.

v. **AEC175** (*sacA*::P_{spoIID}-*yfp Cm*^{R}) – The 232bp upstream of *spoIID* start codon were introduced between the EcoRI and BamHI sites of AEC127.

vi. **AEC247** (*sacA*::P_{spoIIQ}-*yfp*) – The 140bp upstream of *spoIID* start codon were introduced between the EcoRI and BamHI sites of AEC127.

vii. **AEC334** (*sacA*::P_{gerE}-*yfp Cm*^{R}) – 184bp fragment upstream of the *gerE* gene was cloned into AEC127 using EcoRI and BamHI.

viii. **AEC336** (*sacA*::P_{sspA}-*yfp Cm*^{R}) – 234bp fragment upstream of the *sspA* gene was cloned into AEC127 using EcoRI and BamHI.

ix. **AEC277** (*amyE*:3×yfp). We constructed an integration plasmid based on pLD30 (*amyE*::*Spec*^{R} integration vector[2]) in which 3 separate copies of *yfp*, each with its own RBS are flanked by terminators. A multiple cloning site was inserted before the first *yfp* for introducing the promoter of choice using EcoRI and BamHI restriction sites.

x. **AEC279** (*amyE*::P_{spoIIR}-3×yfp *Spec*^{R}). The 200bp upstream of *spoIIR* were ligated into the EcoRI and BamHI ites of AEC277.

xi. **AEC278** (*amyE*::P_{spoIIQ}-3×yfp *Spec*^{R} integration plasmid). The 200bp upstream of *spoIIQ* were ligated into the EcoRI and BamHI sites of AEC277.

xii. **AEC344** (*ppsB*::*spoIIR*;P_{spoIIR}-3×yfp *Neo*^{R}) P_{spoIIR}-3×yfp was amplified from AEC279 with flanking restriction sites XXX,XXX and ligated into the corresponding sites in pVK325. The direction of the reporter is opposite to the direction of the *spoIIR* gene in a converging manner.

xiii. **AEC308** (*amyE*::$P_{spoIIElacO}$-*mCherry* lacI *Spec*^{R}): The hyper-spank promoter of pDR111 (gift from David Rudner, Harvard Medical School) was replaced by a *spoIIE* promoter that included a lacO binding site 2 base pairs downstream of the predicted -10 σ^A binding site (see full sequence of the promoter in Fig. S12). A ribosome binding site and a codon optimized version of *mCherry* as well as two terminators (from *rrnB* and *trpA* [3]), were incorporated at the vector's multiple cloning site using SalI and sphI restriction sites.

xiv. **AEC309** (*spoIIE*-RBS-*mCherry*Ω*spoIIE*). *mCherry* and its RBS were ligated into pKL147[4] between the XhoI and sphI site. A 1kbp fragment of *spoIIE* was subsequently cloned upstream of the RBS into the EcoRI and XhoI sites.

xv. **AEC363** (*amyE*::$P_{spoIIRlacO}$-*mCherry* lacI *Spec*^{R}). The *spoIIE* promoter of AEC308 was replaced with a version of *spoIIR* promoter containing a lacO binding site 1bp downstream of the -10 σ^F predicted binding site (see full promoter sequence in Fig S3).

xvi. **AEC362** (*amyE*::$P_{spoIIQlacO}$-*mCherry* lacI *Spec*^{R}). The *spoIIE* promoter of AEC308 was replaced with a version of *spoIIQ* promoter containing a lacO binding site 1bp downstream of the -10 σ^F predicted binding site (see full promoter sequence in Fig S3).

xvii. **AEC360** (*amyE*::P_{spoIIR}-*mCherry* lacI *Spec*^{R}). The *spoIIE* promoter of AEC308 was replaced with the same *spoIIR* promoter as in AES363 but without the lacO binding site. Used to calibrate *spoIIR*^{Hypo} expression.

xviii. **AEC365** (*amyE*::$P_{spoIIRlacO}$-*spoIIR-mCherry* lacI *Spec*^{R}) *spoIIR* gene and its RBS were integrated into AEC363 between SalI and ClaI restriction sites forming a bicistronic transcript with *mCherry* – see map of the integration part of the plasmid in Fig. S4.

xix. **AEC364** (*amyE*::$P_{spoIIQlacO}$-*spoIIR-mCherry* lacI *Spec*^{R}) *spoIIR* gene and its RBS were integrated into AEC362between SalI and ClaI restriction sites forming a bicistronic transcript with *mCherry* .

xx. **AEC369** (*amyE*::$P_{spoIIQlacO}$-2xyfp-*spoIIR-mCherry* lacI *Spec*^{R}): 2 copies of *yfp* were inserted into AEC364 restriction site, to form a co-cistronic operon together with spoIIR.

xxi. **AEC375** (ppsB::P_{sigA}-mCherry): σ^A promoter from the trpE gene was fused to mCherry and cloned into the ppsB integration vector, pVK317, replacing the P_{spoIIQ}-spoIIR construct.

***B. subtilis* strains:**

Strains used in the paper were from PY79 or BR151 genetic backgrounds. Antibiotic resistance was switched by using antibiotic switcher vectors [5,6]. The appropriate antibiotic marker is marked but the switching stages are omitted.

	Strain name	Genotype	Construction method (**mutant strain description**)	Used in figure	Reference/source
1	PY79	Prototrophic strain			[7]
2	AES406	PY79;*spoIIR*::Kan	RL1063 (**Δ*spoIIR***)	Fig. 3c (Filled circle)	JD lab stock
3	Jdb1153	PY79;*amyE*::P_{spoIIQ}-*cfp Spec*^{R}	Integration of pKM8 into PY79, Bs. codon optimized *cfp*		[8]
4	AES544	PY79;*amyE*::P_{spoIIQ}-*cfp Spec*^{R};*sacA*::P_{spoIID}-*yfp Cm*^{R}	AEC175→jdb1153	Fig. S1b	This work
5	AES516	PY79;*spoIIR*::*Neo*^{R}; *ppsB*::P_{spoIIQ}-*spoIIR Erm*^{R}	AEC326→AES406 (***spoIIR*^{delay}**)	Figs. 3c (filled square),3e, 4b,S4c, S8a,S9	This work
6	AES525	PY79;*spoIIR*::*Neo*^{R}; *ppsB*::P_{spoIIQ}-*spoIIR Erm*^{R}; *amyE*::P_{spoIIQ}-*cfp Spec*^{R}	Jdb1153→AES516 (***spoIIR*^{delay}**)		This work
7	AES528	PY79;*spoIIR*::*Neo*^{R}; *ppsB*::P_{spoIIQ}-*spoIIR Erm*^{R}; *amyE*::P_{spoIIQ}-*cfp Spec*^{R} ;*sacA*::P_{spoIID}-*yfp Cm*^{R}	AEC175→AES606 (***spoIIR*^{delay}**)	Figs. 2a-d	This work
8	AES569	PY79;*spoIIR*::*Tet*^{R}; *ppsB*:: *spoIIR Neo*^{R}; *amyE*::P_{spoIIQ}-*cfp Spec*^{R} ;*sacA*::P_{spoIID}-*yfp Cm*^{R}	pVK325→AES528 (***spoIIR*^{distal}**)	Fig. S1a	This work
9	AES606	PY79;*spoIIR*::*Erm*^{R}; *ppsB*::*spoIIR* P_{IIR}-3×yfp *Neo*^{R}	AEC344→AES525 (***spoIIR*^{distal}**)	3c (empty circle),	This work
10	AES607	PY79;*spoIIR*::*Erm*^{R}; *ppsB*::*spoIIR* P_{IIR}-3×yfp *Neo*^{R} ;*amyE*::P_{spoIIQ}-*cfp Spec*^{R}	Jdb1153→AES606 (***spoIIR*^{distal}**)	S2a-d,S4g	This work
11	Jdb651	PY79;*amyE*::TetO (*Cm*^{R} x 5);vegΩP_{veg}-*TetR*-GFP *Erm*^{R}		Fig. S11b	[9]
12	AES558	PY79;*spoIIR*::*Tet*^{R}; *amyE*::TetO (*Cm*^{R} x 5);vegΩP_{veg}-*TetR*-GFP *Erm*^{R}	AES406→jdb651; High level of Cm selected for multiplic*a*tion of TetO cassete		This work
13	AES559	PY79;*spoIIR*::*Tet*^{R}; *amyE*::TetO (*Cm*^{R} x 5);vegΩP_{veg}-*TetR*-GFP *Erm*^{R}; *ppsB*::P_{spoIIQ}-*spoIIR Neo*^{R}	pVK317→AES568; (***spoIIR*^{delay}**)	Fig. 2e	This work
14	SL14341	JH641;*ΔyabA*::*Cm*^{R}	A kind gift of A.		[10,11]

			Grossman		
15	AES618	PY79;*ΔyabA*::*Cm*^{R}	SL14341→PY79 (**Δ*yabA***)	Fig. S11g	This work
16	AES620	PY79; *spoIIR*::*Tet*^{R}; *ppsB*::P$_{spoIIQ}$-*spoIIR Neo*^{R};*ΔyabA*::*Spec*^{R}	(***spoIIR*^{delay};Δ*yabA***)	Fig. 4b	This work
17	AES639	PY79;*spoIIR*::*Tet*^{R}; *amyE*::TetO (*Cm*^{R} x 5);vegΩP$_{veg}$-*TetR*-GFP *Erm*^{R}; *ppsB*::P$_{spoIIQ}$-*spoIIR Neo*^{R};*ΔyabA*::*Spec*^{R}	AES638→AES559 (***spoIIR*^{delay};Δ*yabA;Tet-Dot***)	Figs. S11b,c	This work
18	AES240	*sacA*::P$_{spoIIQ}$-*yfp Cm*^{R}	AEC247→PY79		This work
19	Jdb1	PY79;*spoIIE*::Kan			[12]
20	AES462	PY79;*spoIIE*::Kan;*amyE*::P$_{spoIIE}$$_{lacO}$-*spoIIE*-RBS-Cherry lacI *Spec*^{R}	*spoIIE* was ligated to AEC308 and directly transformed into jdb1 (***spoIIE*^{Hypo}**)		This work
21	AES608	PY79;*spoIIE*::Kan;*amyE*::P$_{spoIIE}$$_{lacO}$-*spoIIE*-RBS-Cherry lacI *Spec*^{R};*spoIIR*::*Tet*^{R};*SacA*::P$_{spoIIQ}$-*yfp Cm*^{R}	AES240→AES462	Figs. 3d, S12e	This work
22	AES467	PY79;*spoIIE*-cherryΩ*spoIIE Tet*^{R}	AEC309→PY79 (single crossover)		This work
23	AES417	PY79; *amyE*::P$_{spoIIE}$$_{lacO}$-*mCherry* lacI *Spec*^{R}	AEC308→PY79	Figs. S12c,d	This work
24	AES666	PY79;*amyE*::P$_{spoIIR}$-*mCherry* lacI *Spec*^{R}; *sacA*::P$_{spoIIQ}$-*yfp Cm*^{R}	AEC360→AES240	Figs. S3c,d	This work
25	AES667	PY79;*amyE*::P$_{spoIIR}$$_{lacO}$-*mCherry* lacI *Spec*^{R}; *sacA*::P$_{spoIIQ}$-*yfp Cm*^{R}	AEC363→AES240	Figs. S3c,d	This work
26	AES673	PY79; *spoIIR*::*Tet*^{R}; *amyE*:: P$_{spoIIR}$$_{lacO}$ -*spoIIR-mCherry Spec*^{R}; *sacA*::P$_{spoIIQ}$-*yfp Cm*^{R}	AEC365 →AES240; ***spoIIR*^{Hypo}**	Figs. 3c (empty diamond, 3uM IPTG, empty star, 6uM IPTG), S3e	This work
27	MZ50	PY79;*spoIIR*::*Neo*^{R}; zdd-85::*spoIIR*(123°) *Spec*^{R}	***spoIIR*^{distal1}**	Fig. 3c (filled diamond)	[13]
28	MZ49	PY79;*spoIIR*::*Neo*^{R}; zce-82::*spoIIR*(94°) *Spec*^{R}	***spoIIR*^{distal2}**	Fig. 3c (empty square)	[13]
29	AI109	JH642;spo0J-GFP			[14]
30	AES546	PY79; *amyE*::P$_{spoIIQ}$-*cfp Spec*^{R} ;spo0J-GFP *Cm*^{R}	AI109 →jdb1153 (**spo0J-GFP**)	Fig. S11b,f	This work
31	AES548	PY79;*spoIIR*::*Neo*^{R}; *ppsB*::P$_{spoIIQ}$-*spoIIR Erm*^{R} *amyE*::P$_{spoIIQ}$-*cfp Spec*^{R} ; spo0J-GFP *Cm*^{R}	AI109 →AES525 (***spoIIR*^{delay};spo0J-GFP**)	Fig. 4a,S11d,e	This work
32	Jdb404	PY79;zae-			[12]
		86::Tn917::pTV21Δ2::pD177.1:: pD179.1 kanR *cat*R spoIIAA+ IIAB1 IIAC(VA233)Ωerm			
33	Jdb434	PY79; zdd-85::Tn917::pTV21Δ2::pD177.1:: pD179.1 kanR cmR			JD lab stock

34	AES652	PY79;zae-86::Tn917::pTV21Δ2::pD177.1::P_{spoIIR}-3×yfp *Spec^R Cm^R*	AEC279→jdb404		This work
35	AES653	PY79;*amyE*::P_{spoIIQ}-*cfp Spec^R*; zae-86::Tn917::pTV21Δ2::pD177.1::P_{spoIIR}-3×yfp *Spec^R Cm^R*	AES652→jdb153	Figs. S2h-j	This work
36	AES434	PY79;*amyE*::P_{spoIIR}-3×yfp *Spec^R*	AEC279→PY79	Figs. S4a,b	This work
37	AES433	PY79;*amyE*::P_{spoIIQ}-3×yfp *Spec^R*	AEC278→PY79	Figs. S4a,b	This work
38	AES574	PY79;*spoIIR*::*Neo^R*; *ppsB*::P_{spoIIQ}-*spoIIR Erm^R*; *amyE*::P_{spoIIQ}-*cfp Spec^R*;*sacA*::P_{sspA}-*yfp*	AEC336→AES525 (***spoIIR^{delay}***)	Fig. S8a	This work
39	AES575	PY79;*spoIIR*::*Neo^R*; *ppsB*::P_{spoIIQ}-*spoIIR Erm^R*; *amyE*::P_{spoIIQ}-*cfp Spec^R*;*sacA*::P_{gerE}-*yfp*	AEC334→AES525 (***spoIIR^{delay}***)	Fig. S8b	This work
40	AES852	PY79;ppsB::PtrpE-Cherry Erm;*spoIIR*::Tet;amyE::P_{spoIIQ}-CFP	AEC375, jdb1153→AES514		This work
41	AES840	PY79; zdd-85::Tn917::pTV21Δ2::pD179.1 kanR $P_{IIQlacO}$-2×*yfp-spoIIR-mCherry Spec^R*	AEC369→jdb434 (**$P_{spoIIQlacO}$-*spoIIR*@124^o**)		This work
42	AES853	PY79;ppsB::PtrpE-Cherry Erm;*spoIIR*::Tet;amyE::P_{spoIIQ}-CFP; zdd-85::Tn917::pTV21Δ2::pD179.1 kanR $P_{spoIIQlacO}$-2×*yfp-spoIIR-mCherry Spec^R*	AES840→AES852 (**spoIIR^{PP-CY}**)	Fig. 3a,b, Fig. S5b	This work
43	SW171	rsfA::Tet			[15]
44	AES629	PY79;*spoIIR*::Erm;ppsB::PIIR-IIR PIIR-3xY Neo;amyE::P_{spoIIQ}-CFP;rsfA::Tet	SW171→AES607	Fig. S4e	This work
45	AES766	PY79; IIR::Erm;ppsB::PIIR-IIR Neo;rsfA::Tet	SW171→AES602	Fig. S4f	This work
46	MF56	PY79; spoIIGB::spoIIGB-GFP Spec			[16]
47	AES765	IIR::Erm;ppsB::PIIR-IIR Neo;spoIIGB::SpoIIGB-GFP Spec	MF56→AES602	Fig. S5c-d	This work
48	Jdb401	amyE::Pspac-ftsZ-GFP			JD lab
49	AES870	IIR::Kan;ppsB::PIIR-IIR Neo;amyE::Pspac-ftsZ-GFP	Jdb401→AES516	Fig. S8d	This work
50	BR151	trpC2 metB10 lys-3			[17]
51	SL14121	BR151; *spoIIR*::*Tet^R*; *ppsB*::P_{spoIIQ}-*spoIIR Neo^R*	(***spoIIR^{delay}***)	Fig. 4b	This work
52	SL14352	BR151;*ΔyabA*	AI109 →BR151 (**Δ*yabA***)		This work
53	SL14363	BR151; *spoIIR*::*Tet^R*; *ppsB*::P_{spoIIQ}-*spoIIR Neo^R*; *ΔyabA*	AI109 →SL14117 (***spoIIR^{distal}*; Δ*yabA***)	Fig. 4b	This work

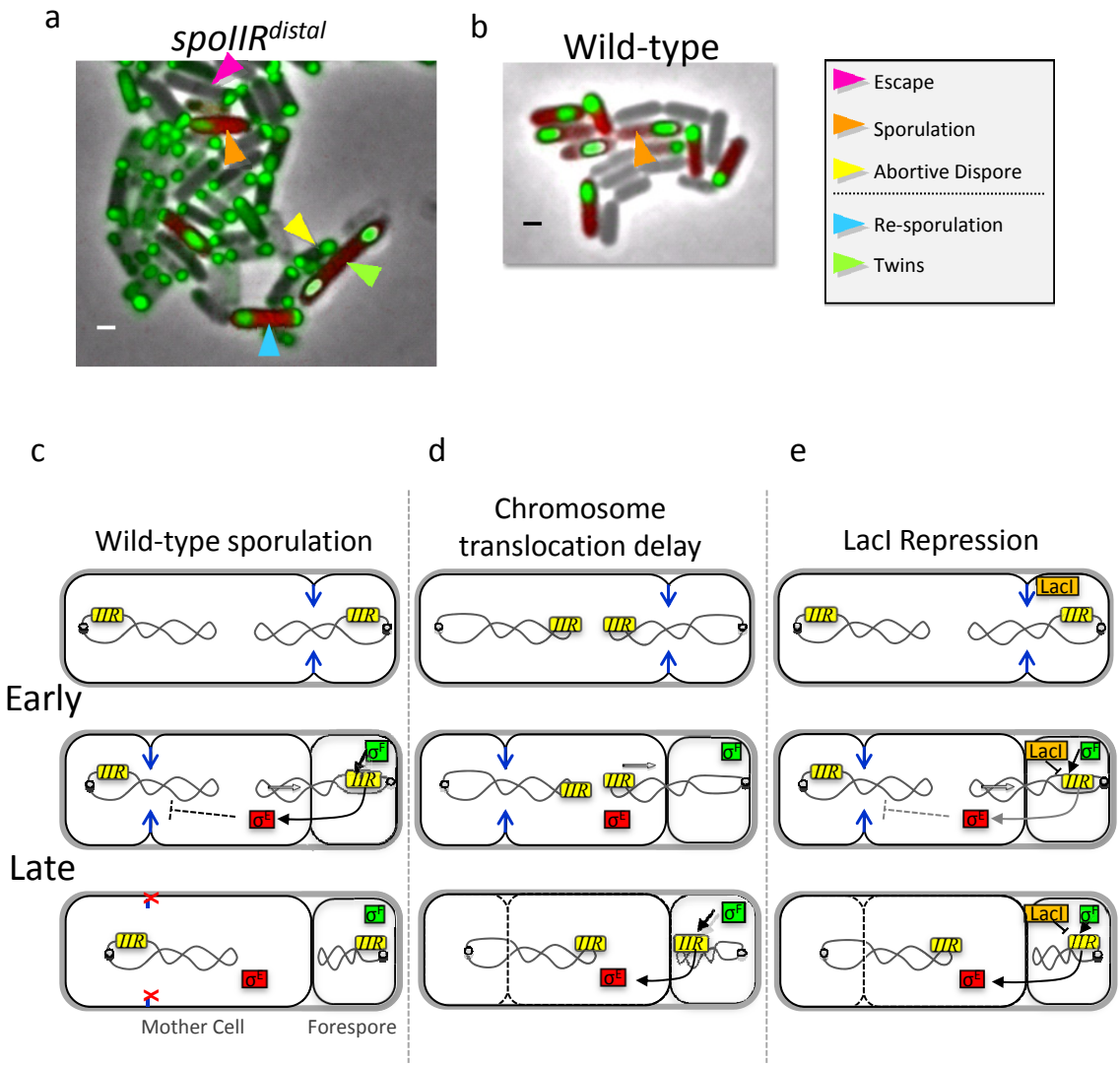

Figure S1. Wild-type and partially penetrant sporulation. (a-b) images of typical microcolonies of (a) *spoIIR*^{PP} (AES569) and (b) wild-type cells. Arrowheads indicate different fates acquired by the cells, as defined in figure. The specific *spoIIR*^{PP} strain shown here is *spoIIR*^{distal}, further described in Fig. S2 and supplementary methods. Scale bar, 1μm. (c-e) Schematic illustration of the two types of mutations used to perturb *spoIIR* expression and allow the expression of a partial penetrance set of phenotypes. (c) Wild-type sporulation: After completion of septation (blue arrows in top, solid line on 'early' and 'late' cartoons), σ^F is activated specifically in the forespore. It transcribes *spoIIR* which in turn leads to activation of σ^E in the mother-cell by cleavage of its membrane bound pro-domain. σ^E target genes in turn block completion of a second asymmetric septum (blue arrows) in mother cell. Concurrently, the distal part of the forespore chromosome (gray line) is translocated into the forespore (white arrow). Origins of replication on the two chromosomes are indicated schematically by gray dots. (d) Chromosome translocation delay mutants. In these strains, the *spoIIR* gene is moved to a distal location. Its expression is controlled either by its own promoter, P_{spoIIR}, in the case of *spoIIR*^{distal}, or by a stronger σ^F-controlled promoter, P_{spoIIQ}, in the case of *spoIIR*^{delay}. In both cases, chromosomal position delays *spoIIR* expression due to the need for DNA translocation prior to activation. The delay causes some cells to fail to activate σ^E in a timely fashion, sometimes resulting in a second septum (black dashed line). (e) In LacI-repressed *spoIIR*^{hypo} mutants, a lac operator is inserted in the *spoIIR* promoter, resulting in an effective transcriptional "AND" gate: SpoIIR is expressed only when σ^F is active and LacI is induced by IPTG (not shown). This reduces the rate of expression of *spoIIR* in an IPTG-dependent manner, without affecting the time at which *spoIIR* is first expressed. Consequently, the activation of σ^E is reduced, or eliminated, leading to the same spectrum of fates observed in *spoIIR*^{delay} mutants. Figure S2 further characterizes the delay mutants, while Figure S3 further characterizes the LacI repression mutants, and Figure S4 characterize their interaction and the interaction with an additional regulator of *spoIIR*, *rsfA*.

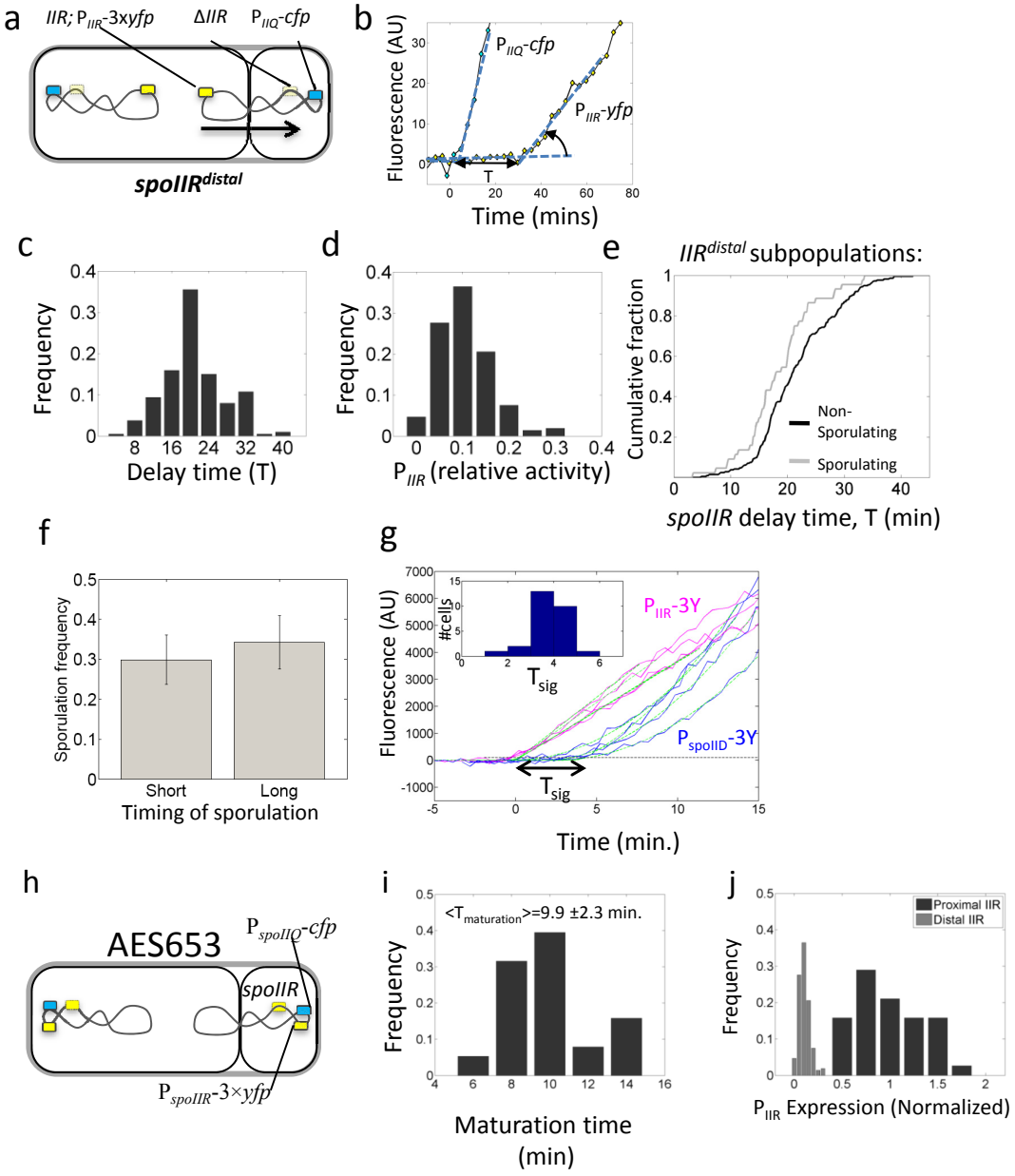

Figure S2. Variability and noise in *spoIIR*^{PP} mutants. (a-d) The strain *spoIIR*^{distal} (AES607) allows analysis of cell-cell variability in *spoIIR* expression. (a) *spoIIR* was moved from its normal position along with a P_{spoIIR}-3×*yfp* reporter cassette (3 tandem copies of *yfp*) to a locus (*ppsB)* near the replication terminus (172°). In this strain, *spoIIR* is not expressed until the *ppsB* locus is translocated into the forespore, creating a delay in the initiation of its expression. Similar mutants, with *spoIIR* inserted at other locations, are also used – see methods for details. This strain also incorporates a P_{spoIIQ}-*cfp* reporter in an *ori*-proximal position (P_{spoIIQ} is activated by σ^F). See Fig. S4 for more details. (b) Analysis of activation of a single typical *spoIIR*^{distal} cell. Total fluorescence is plotted vs. time for the two reporters shown in (a). The delay time, labeled T, is corrected for differences in fluorescent protein maturation times (see (i)). The expression rates are defined as the slope of total fluorescence over time, and normalized to the expression of the same *yfp* reporter gene inserted at an origin-proximal locus, as shown in (j). (c) Delay time, T, is variable. Histogram over N=250 cells is shown. The delay takes 20 +/- 6 min (mean ± s.d.). (d) Expression rate is reduced to ~10% of its wild-type value, and varies substantially. This histogram is from the same data set as in (c). (e) Correlation between fate and P_{spoIIR} expression. A cumulative histogram of delay time in sporulating (gray) and non-sporulating (black) sub-populations. The

difference between the distributions explains 12% of the variability in this strain. *spoIIR* expression level did not correlate well with fate (not shown). (f) Sporulation timing does not affect fate. Cells of the strain shown in Fig. 3a with sporulation time shorter than the median (denoted Short) and higher than the median (High), sporulated with the same frequency (error bars based on triplicate experiments, std. error). (g) Signaling time, defined as the interval between activation of a P_{spoIIR}-*yfp* reporter in the forespore to the activation of a P_{spoIID}-*yfp* reporter for σ^E activity in the mother cell, is shorter than the chromosomal translocation delay, shown in (c). inset: distribution of signaling times. T_{sig}=3.7±0.9 min (mean ± s.d.). (h) A strain (AES653) in which *spoIIR* and its 3×*yfp* reporter are expressed at proximal positions, so that *cfp* and *yfp* should be activated simultaneously. (i) Analysis of systematic activation time differences in this strain provides a measurement of the difference in maturation times between the two fluorophores. CFP matures 9.9 ± 2.3 min (mean ± s.d.) slower than YFP. (i) Histograms of P_{spoIIR}-3x*yfp* expression in AES653 (black) and $spoIIR^{distal}$ strain (gray, re-plotted from (d)).

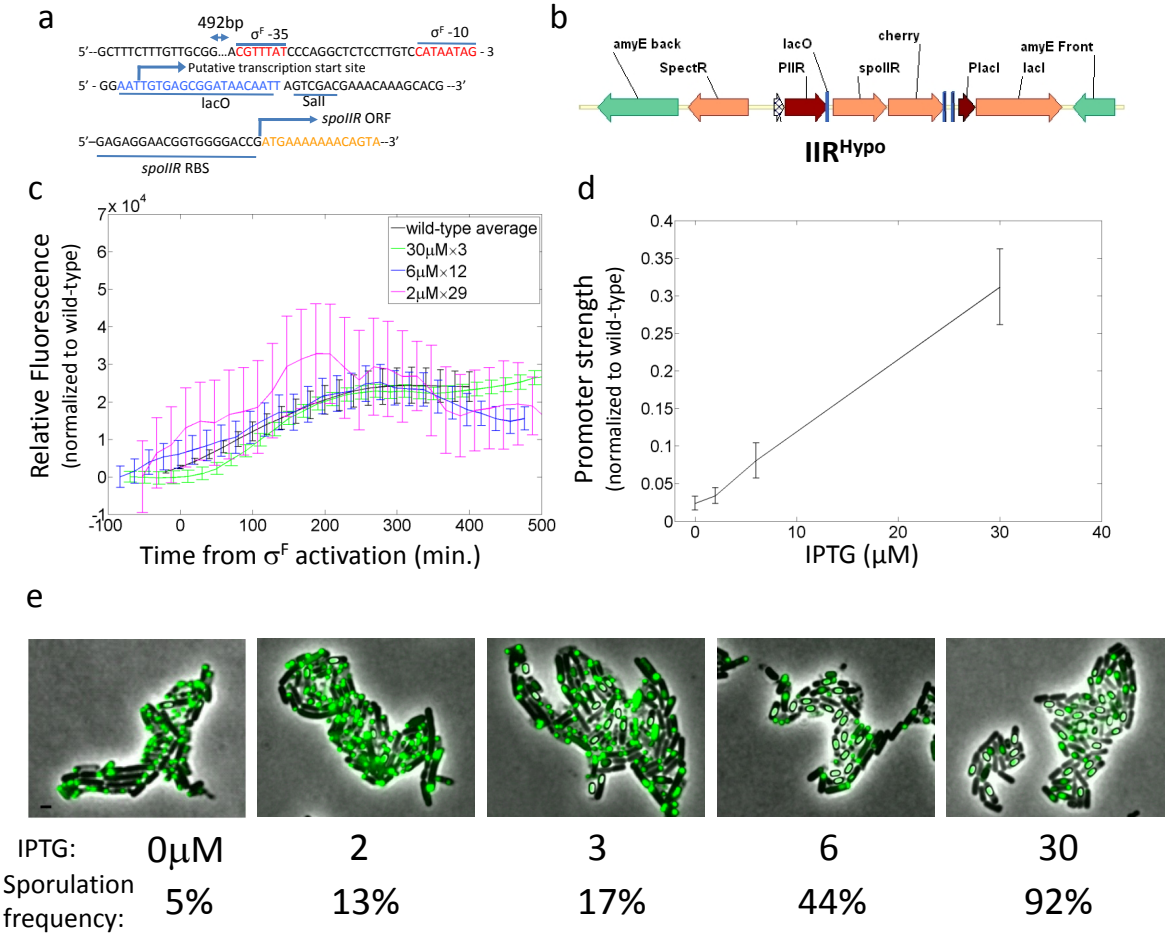

Figure S3. **Construction and single-cell analysis of *spoIIR*^{hypo}.** (a) Sequence of $P_{spoIIRlacO}$ promoter. A lacO binding site and SalI restriction site were inserted 2bp after the σ^F -10 binding site in the parental P_{spoIIR} promoter. (b) Schematic diagram of region integrated at *amyE* with *spoIIR*^{Hypo}. It is based on the integration plasmid pDR111 (provided by D. Rudner, Harvard Medical School). Here, the *spoIIR* gene is expressed under the control of the $P_{spoIIRlacO}$ promoter variant shown in (a), as an operon with the mCherry reporter gene. The vector also enables integration of the *E. coli lacI* gene and appropriate terminators into the same locus. (c-d) $P_{spoIIRlacO}$ expression characterization. (c) A strain containing wild-type *spoIIR* and the $P_{spoIIRlacO}$ promoter driving mCherry (AES667) was analyzed at different IPTG levels using time-lapse microscopy. mCherry levels as a function of time are shown for specific cells, at IPTG levels of 2μM (magenta),6μM (blue) and 30μM (green). Each trace was normalized by its average expression level reduction compared to wild-type, as indicated by multipliers in legend. Also shown is the mean behavior of the parental promoter (lacking the *lac* operator), in strain AES666. (d) Promoter strength was defined as the average mCherry expression levels 200 to 250 minutes after σ^F activation (as measured relative to a P_{spoIIQ}-YFP reporter incorporated into the same strain at a proximal location, not shown). The average promoter strength and its variability (s.d.) are plotted against the wild-type P_{spoIIR} reporter for 4 different concentrations of IPTG. Expression level is approximately linear with IPTG in the range 2-30μM IPTG. 10% of wild-type levels are achieved at ~6 μM IPTG. (e) Sporulation frequency increases with IPTG in images of *spoIIR*^{hypo} colonies (strain AES673). Sporulation frequencies are indicated. Images are composites of phase contrast (gray levels) and P_{spoIIQ}-yfp fluorescent reporter for σ^F activity (green). Scale bar, 1μm.

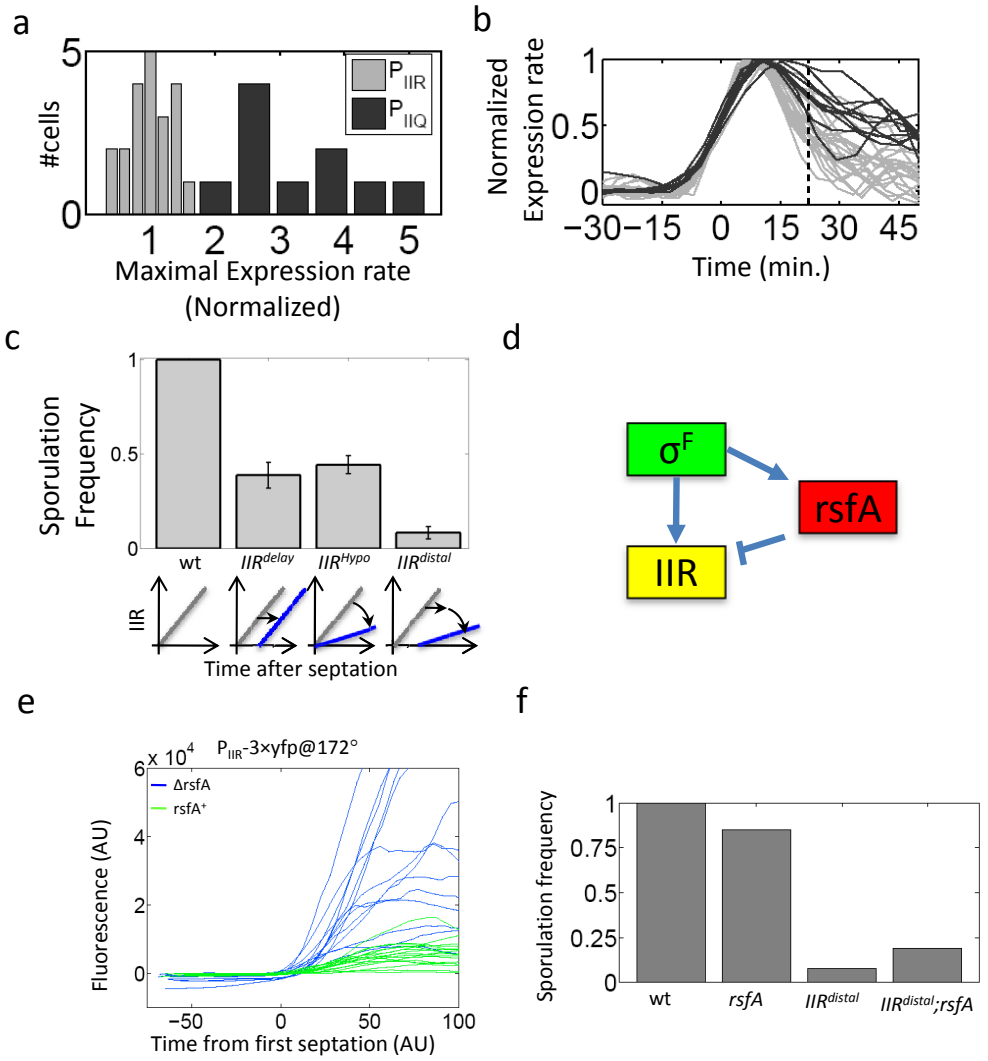

Figure S4. **Interactions between delay and reduction in *spoIIR* expression.** (a-b) Comparison of P_{spoIIR}-*3×yfp* (AES433) and P_{spoIIQ}-*3×yfp* (AES434) expression using single cell analysis of time-lapse movies. Both reporters are integrated in an *ori*-proximal position (at *amyE*) (a) Histograms of maximal P_{spoIIQ} and P_{spoIIR} expression for single cells show that P_{spoIIQ} is ~3 times stronger than P_{spoIIR}. (b) Temporal expression profiles of P_{spoIIR} and P_{spoIIQ} promoters in individual cells. Expression rate is defined as the time derivative of total cellular YFP fluorescence for each cell and curves are smoothed for clarity. All traces are aligned to the onset of expression and normalized by their maximal expression levels. Gray levels as in (a). These data indicate that both P_{spoIIQ} is both stronger and more sustained in its activity than P_{spoIIR}. At the mean translocation time (marked with a vertical dashed line), P_{spoIIQ} expression is two-fold higher than the maximal levels of P_{spoIIR} activity. (c) Comparison of *spoIIR* expression perturbations on sporulation efficiency. Shown are delay only (*spoIIR*^{delay} ,AES516, where *spoIIR* is distally located and controlled by a P_{spoIIQ} promoter), reduction only (*spoIIR*^{hypo}) or combined delay and reduction (*spoIIR*^{distal}). The effects of the two types of perturbations are additive. The type of perturbation (delay and/or reduction in *spoIIR* expression) is diagrammed schematically below the plot. (d-f) RsfA, a regulator of *spoIIR,* affects the behavior of *spoIIR*^{distal} mutants. (d) RsfA was shown to repress *spoIIR* and to be activated by σ^F (ref. [18,19]), forming an incoherent feed-forward loop as indicated[20], . (e) A distal P_{spoIIR}-*yfp* reporter shows enhanced expression in a Δ*rsfA* mutant, as expected. (f) In agreement with this result, the Δ*rsfA* partially rescues the reduction in sporulation efficiency from the *spoIIR*^{distal} mutation.

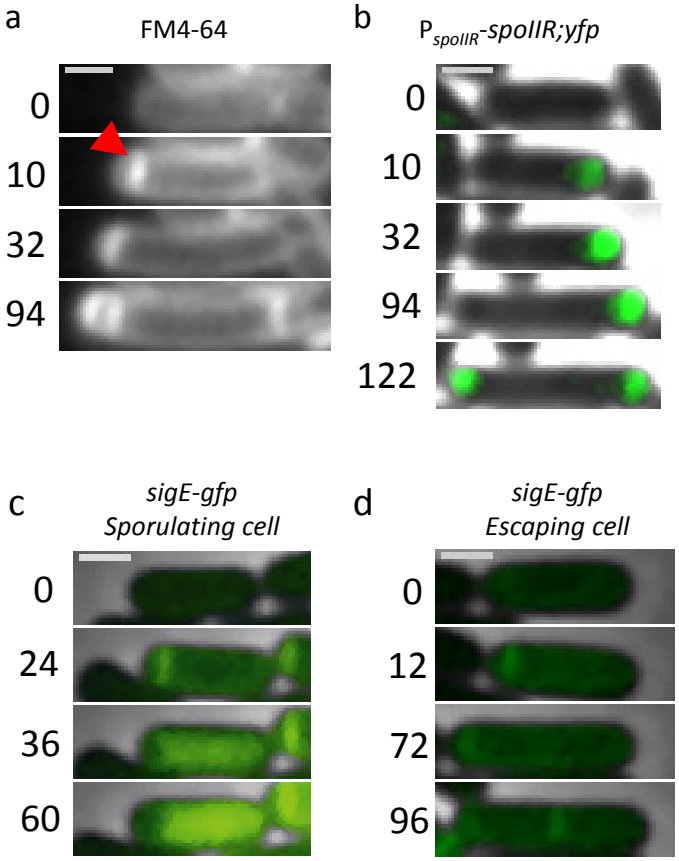

Figure S5. Characterization of sporulation escape. (a) Escaping cells do not generate a second septum at the opposite pole. This FM4-64 time-lapse filmstrip shows a cell that forms a single forespore compartment (red arrow on second image) and then continues to grow (escapes) without making more compartments (compare second to third image). Finally, the cell makes two compartments and continues to form a twin cell (not shown). (b) SpoIIR is expressed in the forespore of an escaping cell. Shown is the expression of YFP (colored green), co-expressed with *spoIIR* in an operon in a typical cell (strain AES853). The final frame shows re-initiation of sporulation with a new forespore. (c,d) Pro-σ^E cleavage in mono-sporulating (c) and escaping (d) cells. We used a SigE-GFP fusion to follow the localization of σ^E protein in a *spoIIR*^{PP} mutant (AES765). (c) In a cell that continues with sporulation, SigE-GFP is initially membrane bound[16]. Following *spoIIR* expression its membrane pro-domain is cleaved and it is released to the cytoplasm[21] (compare second and third images in (c)). (d) sigE-GFP was never seen to become cytoplasmic in the escaping sub-population of the same strain as (c). Time in each filmstrip is indicated in minutes from first frame. Scale bar, 1μm.

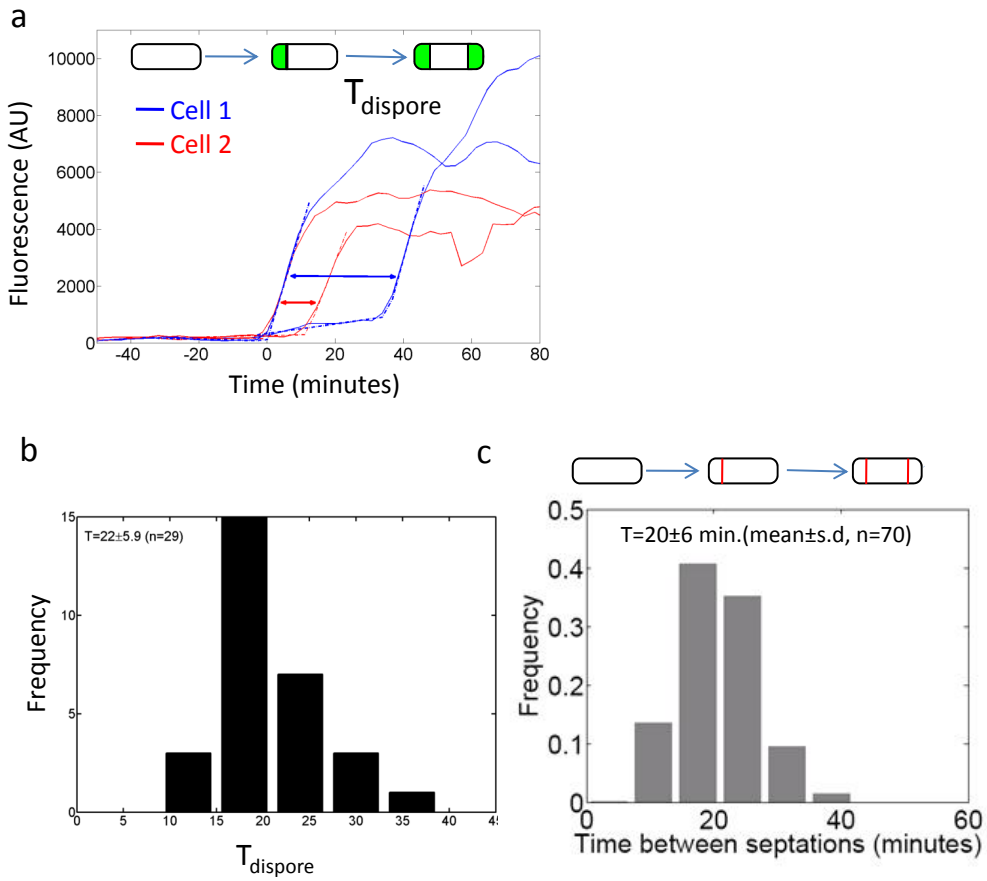

Figure S6. **Time interval between formation of two asymmetric septa in abortive disporic cells.** (a) The expression of a proximal P_{spoIIR}-*3×yfp* reporter is measured at the two halves of the cell. Shown are time traces for two cells (one in magenta and the other in blue). The time between onset of activation of the two forespores varies substantially. In some cases (not shown), P_{spoIIR} levels may also vary substantially between forespores. (b) Distribution of the time interval between the formation of the two septa. (c) Monitoring abortive disporic cells with the membrane stain FM4-64 yielded similar results. The time between formation of the two septa in the twin was found to be similar to that observed in the dispore (not shown).

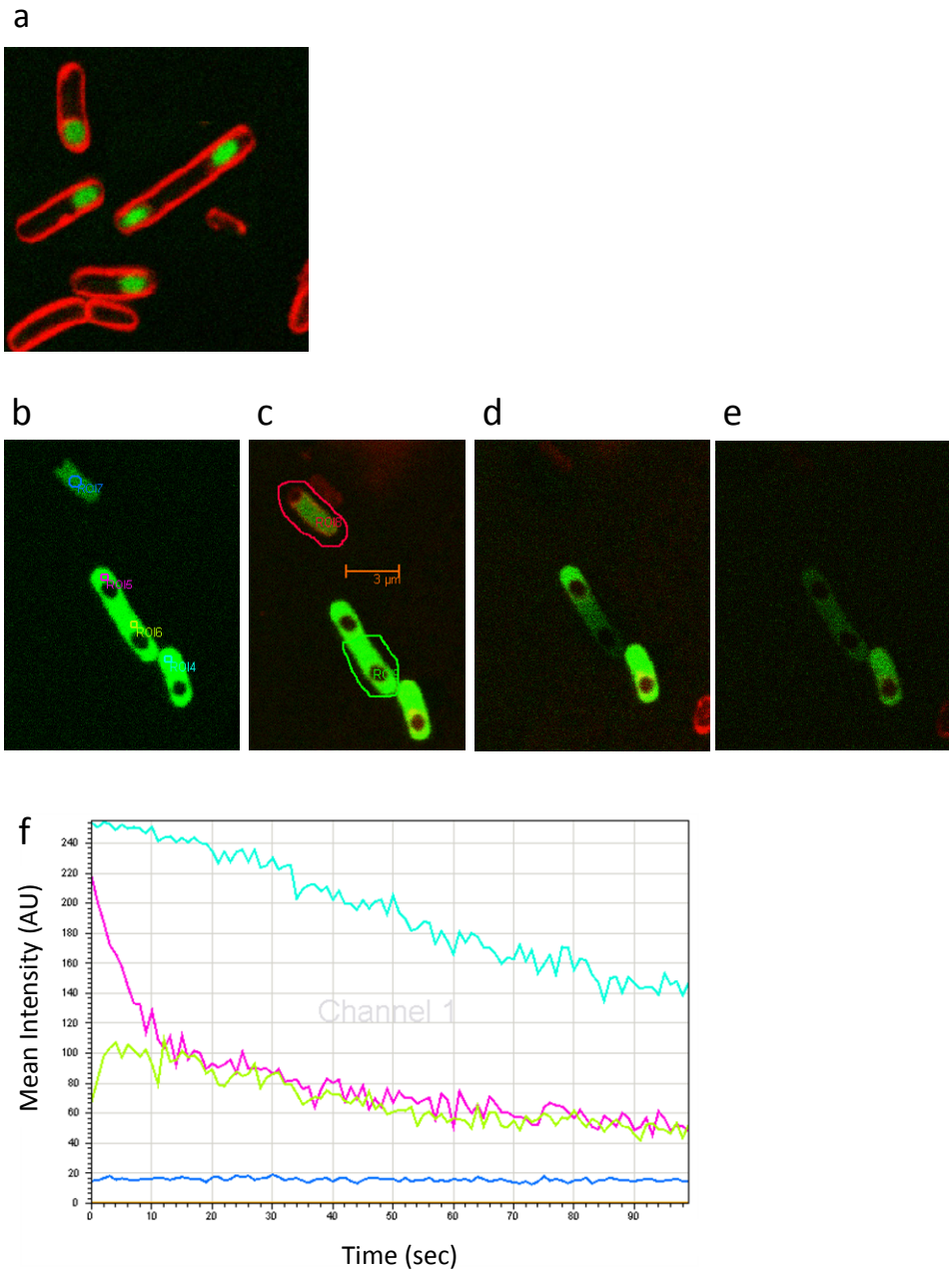

Figure S7. The twin mother-cell is a single compartment. (a) Membrane marker (FM4-64, red) does not show any sign of staining within the mother-cell of a twin-forming cell. Forespores are marked with a P_{spoIIQ}-*gfp* reporter. (b-f) Fluorescence recovery after photobleaching (FRAP) experiments demonstrate that the mother-cell is a single compartment. (b) Fluorescece levels were followed during a FRAP experiment as indicated by colored regions of interest (ROIs). ROI 5,6 (magenta and green respectively) monitor fluorescence level within the same cell. (c) 2/3 of the twin's area was bleached. Marked are areas designated for bleaching. ROI6 is within the area and ROI5 is outside it. (d,e) Images of the cells immediately after photobleaching (d) and 100 seconds later (e). (f) Quantification of fluorescence levels in all ROIs (color corresponds to that in (b)). Note that fluorescence level between the two twin's ROIs equilibrates within ~10 seconds corresponding to a diffusion coefficient of ~2.5um^2/sec, comparable to previously measured cytoplasmic diffusion rates in bacterial cells[22]. Controls: ROI4 is an unbleached cell, while ROI7 is an entirely bleached cell.

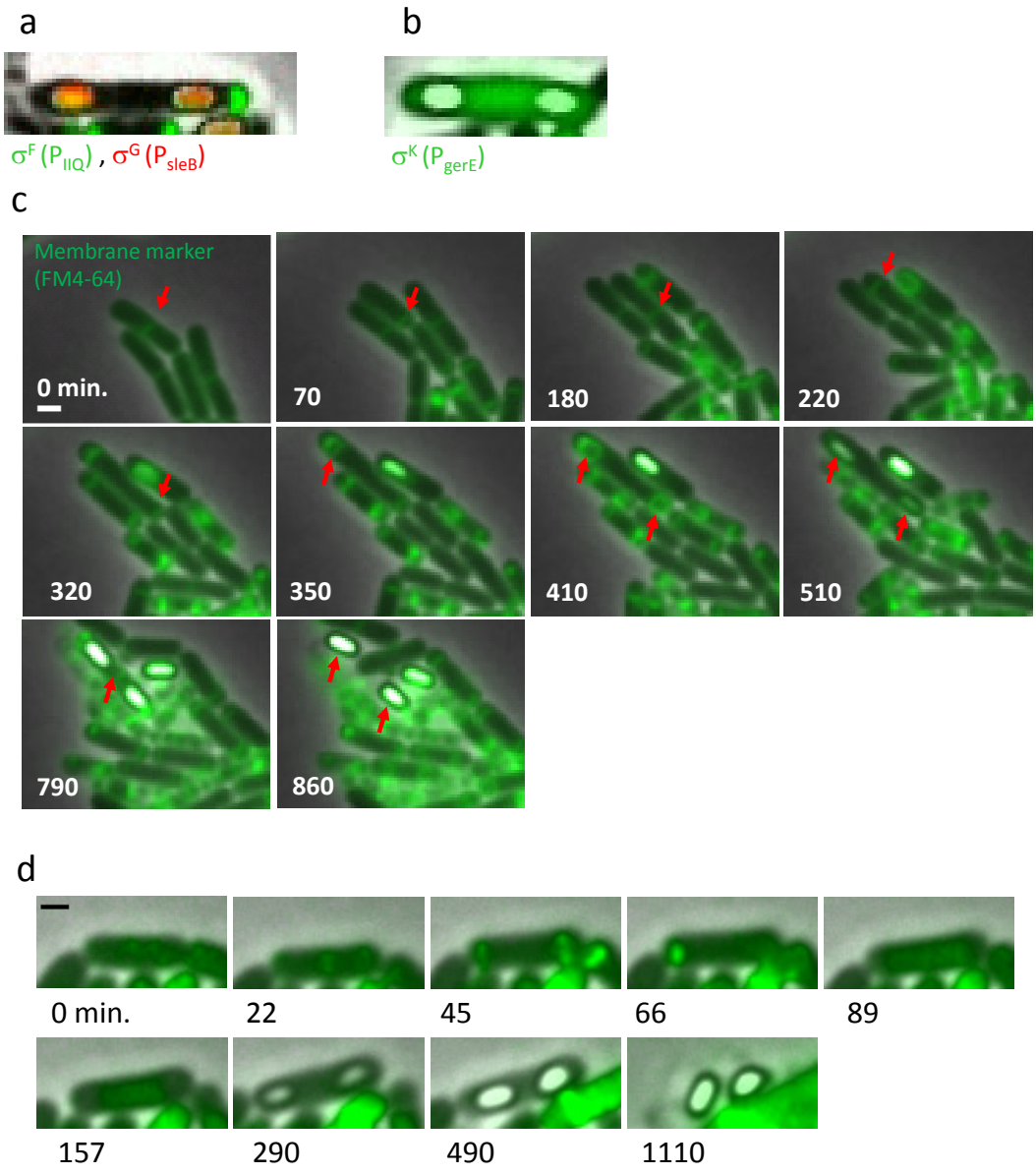

Figure S8. Characterization of twins. (a,b) Twins activate late sporulation sigma factors. Shown are (a) σ^F (green, P_{spoIIQ}-CFP) and σ^G (red, P_{sleB}-YFP) reporters (AES574). Note that the forespore formed prior to escape (right pole) appears green as it activates σ^F, but does not develop further. (b) σ^K reporter (green, P_{gerE}-*yfp*) (AES575), showing that σ^K is expressed in twins as expected. (c) A filmstrip of twin formation in a *spoIIR*^{delay} mutant, with an FM4-64 membrane marker shown in green and phase contrast images in gray. Division events occurring between the last vegetative division and formation of two mature spores are indicated: the final vegetative division (0 min); 1st asymmetric division (70); escape and a vegetative-like division (180); failed asymmetric division (220); 1st twin asymmetric division (320); 2nd twin asymmetric division (350); engulfment (410); phase bright spores (510); mother-cell lysis (790); two mature spores (860). (d) Twin spore-formers do not form an ftsZ ring after the formation of both forespores. An IPTG inducible ftsZ-GFP reporter (AES870) was inserted into a spoIIR^{delay} mutant. The induction of ftsZ-GFP by 20μM of IPTG led to a marked reduction in twin frequency (<0.1% of sporulating cells). The few twins that were formed during a time-lapse movie of sporulating cells did not show any ftsZ ring in the mother-cell after the formation of the twin forespores. Shown is a film strip of a twin sporulating cell showing ftsZ-GFP expression (green) and phase contrast image (gray). Time is indicated in minutes. Scale bar, 1μm.

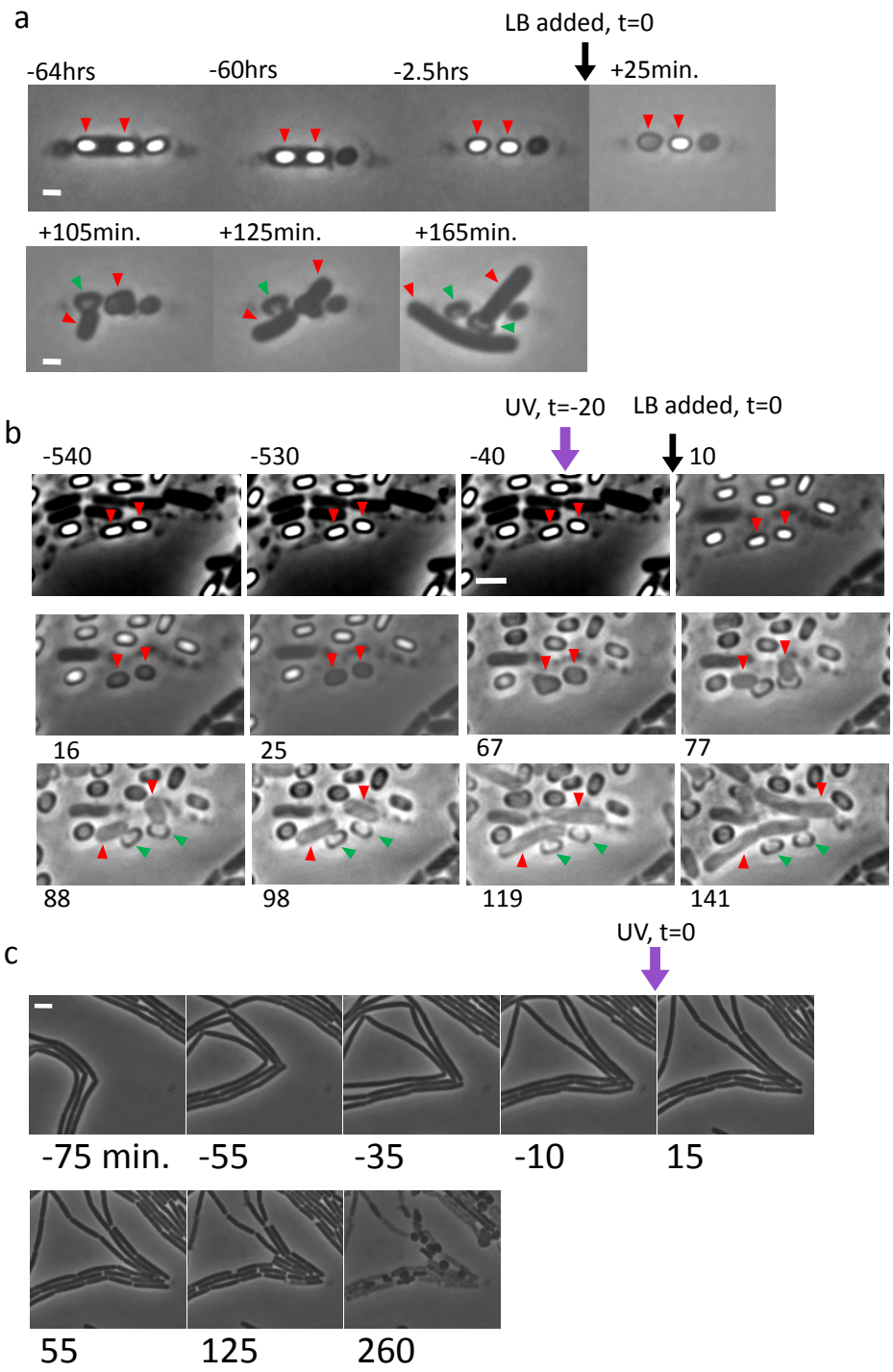

Figure S9. Germination and UV-resistance of twins. (a) Twin spores re-grow upon addition of growth medium. *spoIIR*^{delay}*;spo0J-GFP* cells (AES548) were induced for sporulation using time-lapse conditions (see methods) and were followed until spores matured throughout the agarose pad. 8µl of LB was then added to the pad. Shown is a filmstrip, where twin spores form and mature. Both twin spores germinated and re-grew upon addition of LB similarly to mature monospores. Red arrowhead marks the two spores of the twin. After germination of the cell from the spore, an empty spore shell is retained in place. The green arrowhead marks the appropriate spore shells in cases where it may cause confusion. Scale bar, 1µm. (b,c) Twin spores are resistant to UV irradiation. Filmstrips of sporulating twin spores (b) and vegetative cells (c) that were exposed to 10 seconds of UV irradiation from an unfiltered Xenon lamp. (b) 5µl of LB was added to the irradiated spores. In this case, only part of the spore population germinated. Shown is a case where the two twin spores germinated. (c) Control showing that the irradiation was strong enough to kill vegetative cells. Red and green arrows are as in (a). Time is indicated in minutes (unless otherwise noted) from time of addition of LB (a,b) or irradiation by UV (c). Scale bar, 2µm in (b) and 3µm in (c).

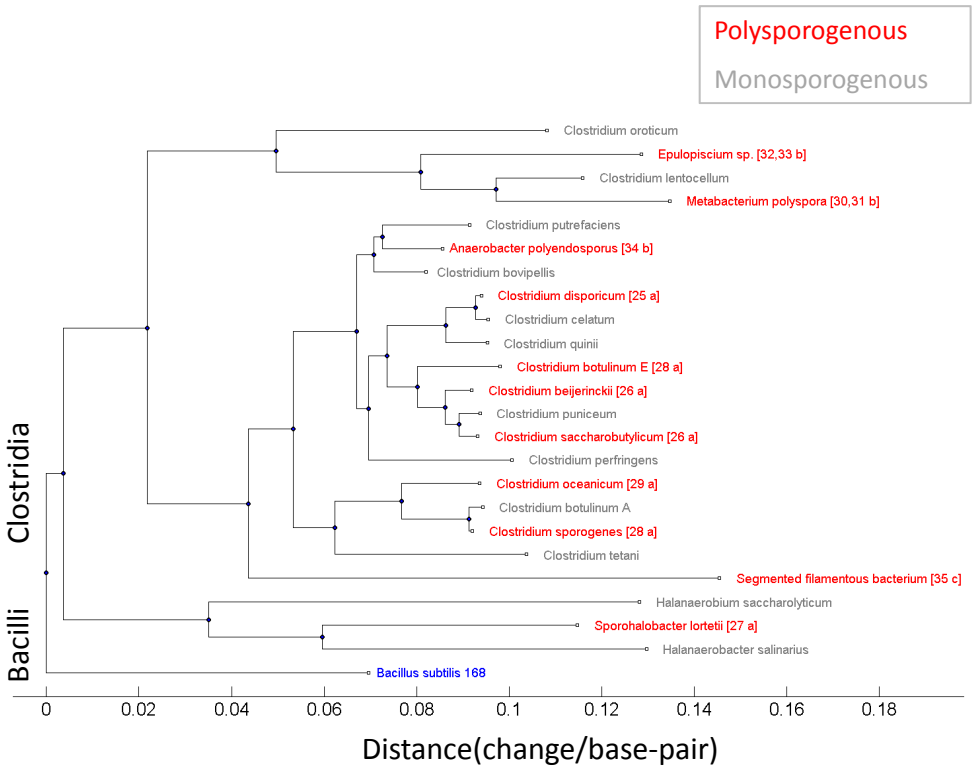

Figure S10 Phylogenetic analysis of species producing multiple endospores (polysporogenous). Shown is a phylogenetic tree including all reported cases (to our knowledge) of polysporogenous species. All known species are in the *Clostridia* class. *Bacillus subtilis* (shown at the bottom) is part of the *Bacilli* class. These two classes of the *firmicutes* diverged about 2.7 Billion years ago[23] but are highly homologous in their sporulation process[24]. Polysporagenous species are sparsely represented among monosporogenous (producing only single endospore) Clostridia species. Some species are strictly twin-like (bi-polar sporulation, marked with *a* in paranthesis)[25-29]. Others may combine bi-polar formation of forespores with forespore binary fission[30-34] to produce more than two spores (marked *b*), or only forespore binary fission[35] (marked *c*). See ref. [36] for further discussion. Phylogenetic tree was made using the Ribosomal Database Project website[37]. References for the specific species are also marked in parentheses.

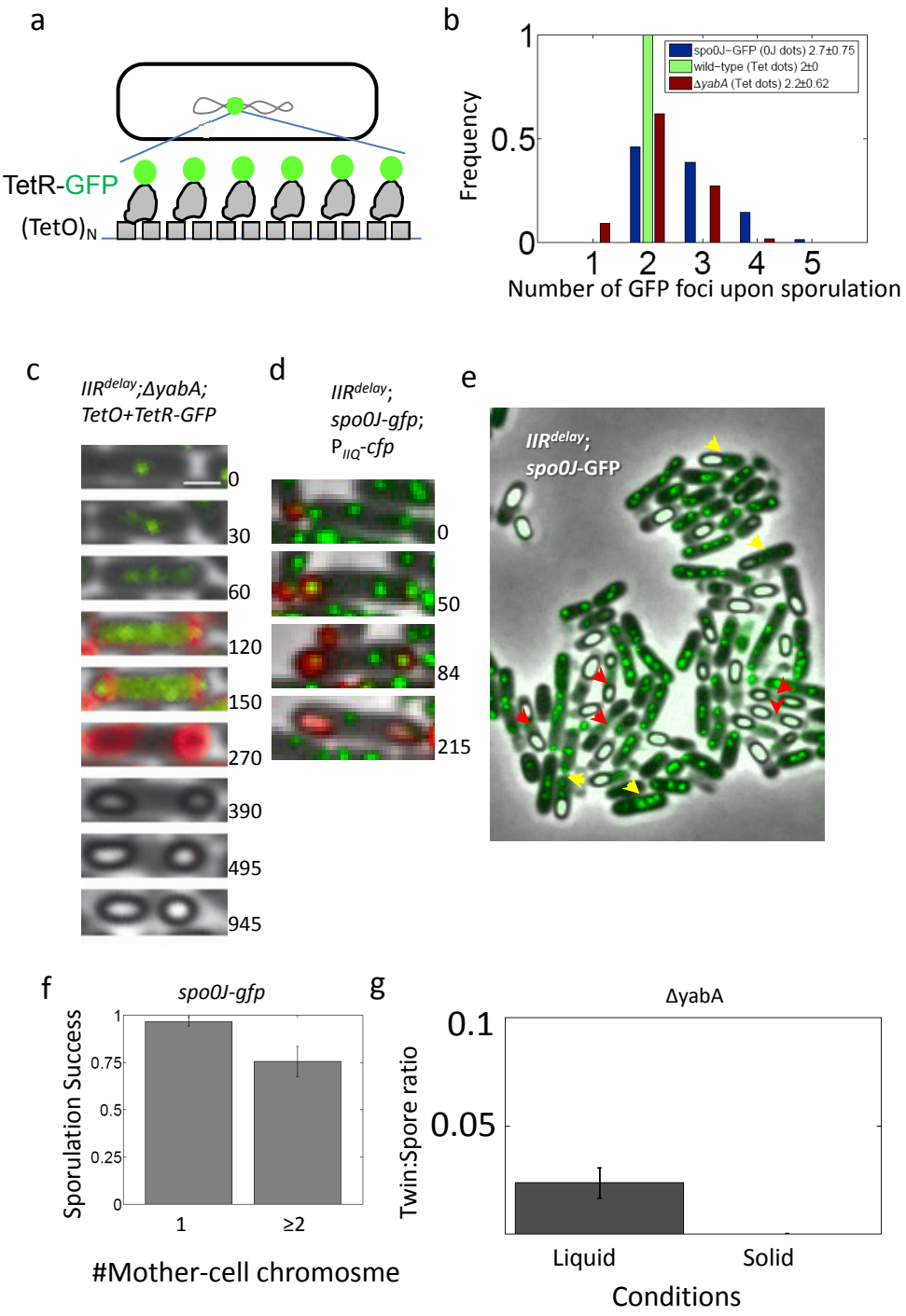

Figure S11. The relation between over-replication and twin formation. (a) To visualize the chromosome, we used a *tetO* cassette inserted into the *amyE* locus (a proximal locus ~30° from the origin of replication). TetR-GFP, expressed under the control of the *veg* promoter, binds to the *tetO* cassette to form a bright localized GFP "dot". (b) The distribution of chromosomal GFP dot number prior to formation of the first septum (as determined from FM4-64 staining in a time-lapse movie). Shown are the distributions of TetR-GFP dots in an otherwise wild-type (green) and Δ*yabA* (red) strains. Sporulation was assayed by FM4-64 stain showing asymmetric division (see methods). *spo0J*-GFP (blue) forms a GFP chromosomal dot by binding to its endogenous binding sites. Sporulation was assayed in this case by the activation of P_{spoIIQ}-*cfp* in the forespore. In the *ΔyabA* strain, dot number is estimated from cells in which dots could be resolved; in ≈70% of the cells no discernible dots were observed, possibly introducing a bias. (c-d) Addition of over-

replication mutation to *spoIIR*^{delay} allows twin formation on the primary sporulation attempt. This is demonstrated in the filmstrips of two strains: *spoIIR*^{delay} combined with Δ*yabA* and a TetR-GFP chromosomal dot system (AES548) (c) and *spoIIR*^{delay} combined with *spo0J*-GFP (AES639) (d). In both cases, vegetative cells with 3 chromosomal dots prior to asymmetric division sporulate to form twins. (c) *spoIIR*^{delay};Δ*yabA* mutant. Phase contrast image in gray, TetR-GFP shown in green (both dots and cytoplasmic/nucleoid background are stained). FM4-64 membrane staining (red) is shown at 120, 150, and 270 minutes to indicate asymmetric septation events and twin sporulation in a single mother-cell. FM4-64 staining was omitted from earlier and later time points for clarity. At later stages of sporulation P_{veg} stops expressing and the TetR-GFP degrades, preventing visualization of dots. (e) A sporulating colony of a *spoIIR*^{delay};spo0J-GFP mutant. Twin sporulating cells are indicated by red arrowheads. Polyploid monospores are indicated with yellow arrowheads. (f) The sporulation success of polyploid mother-cell vs. monoploid (regular) mother-cell was estimated for the two population in a spo0J-GFP mutant, by measuring the fraction of cells that started sporulation and reached the phase bright spore stage. Monoploid success rate is 97% (n=60) while polyploidy success is 75% (n=94). (g) ΔyabA cells show environmental variation in twin formation. We find that in liquid cultures the mutant shows 3% twin:total spore ratio, while in time-lapse conditions virtually no twins were found.

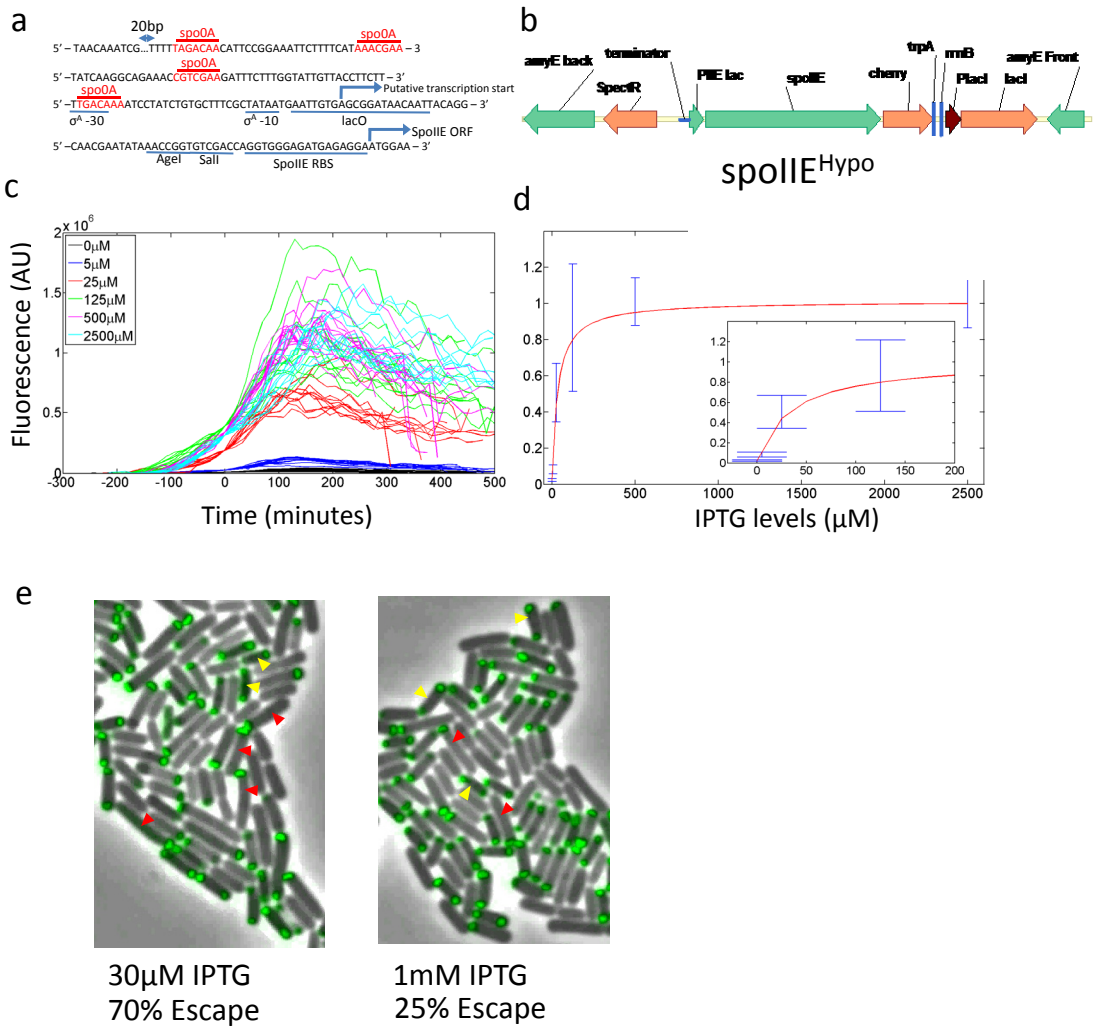

Figure S12. Properties of the *spoIIE*^{hypo} construct. (a) Sequence of the modified P_{spoIIE} promoter, $P_{IIElacO}$. A lacO operator site was added to the promoter 2bp from the σ^A -10 site. Two restriction sites (AgeI and SalI) were introduced further downstream, as shown. A relatively short promoter was used to prevent the inclusion of two neighboring tRNA genes. Binding sites for Spo0A~P, σ^A, and LacI, as well as transcription and translation start sites, are indicated. (b) Structure of the vector used for integrating the *spoIIE*^{Hypo} mutation into the *amyE* site. The vector includes the $P_{spoIIElacI}$ promoter driving *spoIIE* and *mCherry* in an operon. It also includes the *lacI* gene from *E. coli* and appropriate terminators (including *trp* and *rrnB* terminators that were inserted between the gene and *lacI,* not present in the original pDR111 vector). (c) Time traces of individual cells carrying the $P_{spoIIElacO}$ promoter at different concentrations of IPTG (color coded, see figure). Traces are very similar in shape (and in their temporal relation to other sporulation reporters, not shown) but differ in amplitude. Traces are aligned in time so that t=0 is set to the time that cells reach 20% of the average maximal level for the specific induction strength. (d) Promoter strength as a function of IPTG. Strength is calculated as the mean of maximum intensity of individual traces for a given IPTG levels (Error bars are the s.d. of the distribution). The traces are well-fit by a Michaelis-Menten curve with affinity K=34μM, similar to that of $P_{spoIIRlacO}$ and comparable to the known IPTG binding affinity to free LacI. (e) Images of a *spoIIE*^{hypo} mutant carrying a P_{spoIIQ}-*yfp* reporter at two concentrations of IPTG (30μM and 1mM), where sporulation efficiency is close to 100% when signaling is not blocked (not shown). When a signaling null mutation (Δ*spoIIR*) is added, a much higher rate of escape (where the mother-cells grow but do not asymmetrically re-septate) is found in the lower IPTG (≈70% of cells), compared to the higher IPTG (≈25% cells). Examples of escaping (red arrowheads) and abortively disporic (yellow arrowheads) cells are shown in the two images.

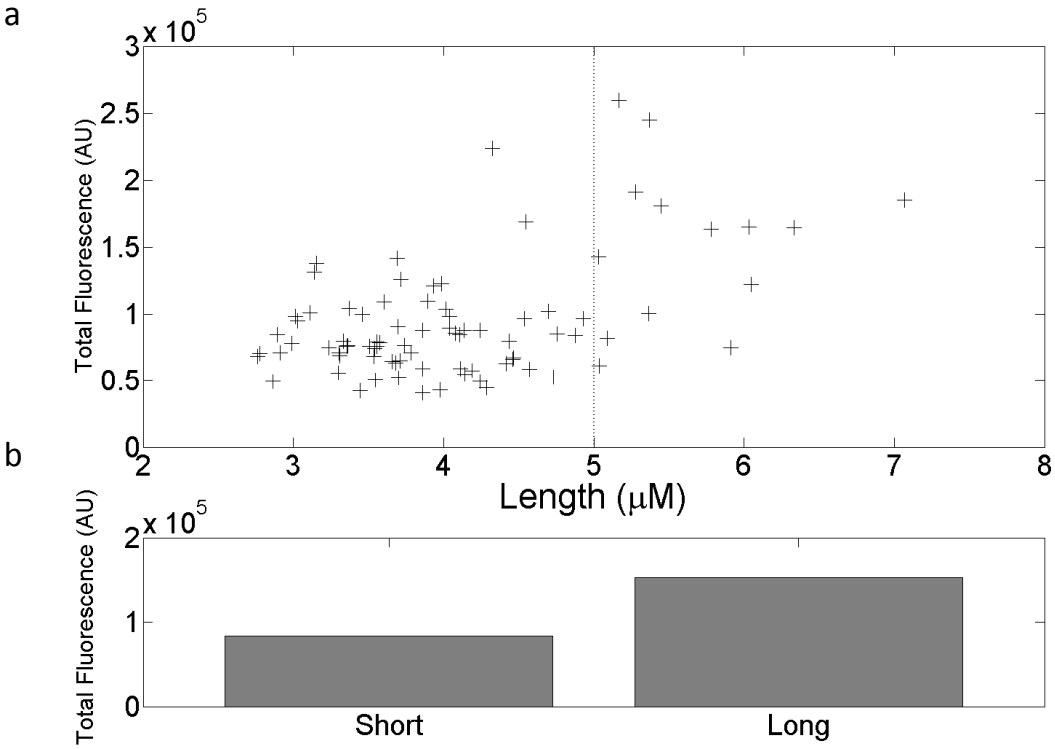

Figure S13. Analysis of DNA content in monosporic *C. oceanicum* cells. Sporulating cells from a liquid culture were placed on an agarose pad with membrane marker (FM4-64 , 2μg/ml) and DNA marker (Vybrant DyeCycle green, 50nM) and imaged. Cells which met the following conditions were analyzed for mother-cell length and DNA content: (1) Only a single forespore by membrane staining, (2) Engulfment process had begun, and (3) The forespore showed marked DNA stain, indicating that DNA translocation was completed on nearly so. (a) A two dimensional plot of total mother-cell DNA fluorescence vs mother-cell's length. A small subpopulation (~10%) of cells are both longer and have higher total fluorescence (right of dashed line). (b) Cells were grouped into two groups with lengths shorter or longer than 5μm (dashed line in (a)). Mean fluorescence of the shorter cells was about half that of the longer cells, consistent with the possibility that the long cells are polyploid.

1. Middleton, R. & Hofmeister, A. New shuttle vectors for ectopic insertion of genes into Bacillus subtilis. *Plasmid* **51**, 238-45 (2004).
2. Garsin, D.A., Paskowitz, D.M., Duncan, L. & Losick, R. Evidence for common sites of contact between the antisigma factor SpoIIAB and its partners SpoIIAA and the developmental transcription factor sigmaF in Bacillus subtilis. *J Mol Biol* **284**, 557-68 (1998).
3. Suel, G.M., Garcia-Ojalvo, J., Liberman, L.M. & Elowitz, M.B. An excitable gene regulatory circuit induces transient cellular differentiation. *Nature* **440**, 545-50 (2006).
4. Lemon, K.P. & Grossman, A.D. Localization of bacterial DNA polymerase: evidence for a factory model of replication. *Science* **282**, 1516-9 (1998).
5. Steinmetz, M. & Richter, R. Plasmids designed to alter the antibiotic resistance expressed by insertion mutations in Bacillus subtilis, through in vivo recombination. *Gene* **142**, 79-83 (1994).
6. Chary, V.K., Amaya, E.I. & Piggot, P.J. Neomycin- and spectinomycin-resistance replacement vectors for Bacillus subtilis. *FEMS Microbiol Lett* **153**, 135-9 (1997).
7. Youngman, P., Perkins, J.B. & Losick, R. Construction of a cloning site near one end of Tn917 into which foreign DNA may be inserted without affecting transposition in Bacillus subtilis or expression of the transposon-borne erm gene. *Plasmid* **12**, 1-9 (1984).
8. Doan, T., Marquis, K.A. & Rudner, D.Z. Subcellular localization of a sporulation membrane protein is achieved through a network of interactions along and across the septum. *Mol Microbiol* **55**, 1767-81 (2005).
9. Dworkin, J. & Losick, R. Does RNA polymerase help drive chromosome segregation in bacteria? *Proc Natl Acad Sci U S A* **99**, 14089-94 (2002).
10. Noirot-Gros, M.F. et al. An expanded view of bacterial DNA replication. *Proc Natl Acad Sci U S A* **99**, 8342-7 (2002).
11. Noirot-Gros, M.F. et al. Functional dissection of YabA, a negative regulator of DNA replication initiation in Bacillus subtilis. *Proc Natl Acad Sci U S A* **103**, 2368-73 (2006).
12. Dworkin, J. Transient genetic asymmetry and cell fate in a bacterium. *Trends Genet* **19**, 107-12 (2003).
13. Zupancic, M.L., Tran, H. & Hofmeister, A.E. Chromosomal organization governs the timing of cell type-specific gene expression required for spore formation in Bacillus subtilis. *Mol Microbiol* **39**, 1471-81 (2001).
14. Lin, D.C., Levin, P.A. & Grossman, A.D. Bipolar localization of a chromosome partition protein in Bacillus subtilis. *Proc Natl Acad Sci U S A* **94**, 4721-6 (1997).
15. Eichenberger, P. et al. The program of gene transcription for a single differentiating cell type during sporulation in Bacillus subtilis. *PLoS Biol* **2**, e328 (2004).
16. Fujita, M. & Losick, R. An investigation into the compartmentalization of the sporulation transcription factor sigmaE in Bacillus subtilis. *Mol Microbiol* **43**, 27-38 (2002).
17. Karow, M.L., Glaser, P. & Piggot, P.J. Identification of a gene, spoIIR, that links the activation of sigma E to the transcriptional activity of sigma F during sporulation in Bacillus subtilis. *Proc Natl Acad Sci U S A* **92**, 2012-6 (1995).
18. Juan Wu, L. & Errington, J. Identification and characterization of a new prespore-specific regulatory gene, rsfA, of Bacillus subtilis. *J Bacteriol* **182**, 418-24 (2000).
19. Wang, S.T. et al. The Forespore Line of Gene Expression in Bacillus subtilis. *Journal of Molecular Biology* **358**, 16-37 (2006).
20. Shen-Orr, S.S., Milo, R., Mangan, S. & Alon, U. Network motifs in the transcriptional regulation network of Escherichia coli. *Nat Genet* **31**, 64-68 (2002).
21. Hilbert, D.W. & Piggot, P.J. Compartmentalization of Gene Expression during Bacillus subtilis Spore Formation. *Microbiol. Mol. Biol. Rev.* **68**, 234-262 (2004).
22. Elowitz, M.B., Surette, M.G., Wolf, P.E., Stock, J.B. & Leibler, S. Protein mobility in the cytoplasm of Escherichia coli. *J Bacteriol* **181**, 197-203 (1999).

23. Battistuzzi, F.U., Feijao, A. & Hedges, S.B. A genomic timescale of prokaryote evolution: insights into the origin of methanogenesis, phototrophy, and the colonization of land. *BMC Evol Biol* **4**, 44 (2004).
24. Paredes, C.J., Alsaker, K.V. & Papoutsakis, E.T. A comparative genomic view of clostridial sporulation and physiology. *Nature Reviews Microbiology* **3**, 969-978 (2005).
25. Horn, N. Clostridium disporicum sp. nov., a Saccharolytic Species Able to Form Two Spores per Cell, Isolated from a Rat Cecum. *Int J Syst Bacteriol* **37**, 398-401 (1987).
26. Keis, S., Shaheen, R. & Jones, D.T. Emended descriptions of Clostridium acetobutylicum and Clostridium beijerinckii, and descriptions of Clostridium saccharoperbutylacetonicum sp. nov. and Clostridium saccharobutylicum sp. nov. *Int J Syst Evol Microbiol* **51**, 2095-103 (2001).
27. Oren, A. Clostridium lortetii sp. nov., a halophilic obligatory anaerobic bacterium producing endospores with attached gas vacuoles. *Archives of Microbiology* **136**, 42-48 (1983).
28. Santo, L.M., Hohl, H.R. & Frank, H.A. Ultrastructure of putrefactive anaerobe 3679h during sporulation. *J Bacteriol* **99**, 824-33 (1969).
29. Smith, L.D. Clostridium oceanicum, sp. n., a sporeforming anaerobe isolated from marine sediments. *J Bacteriol* **103**, 811-3 (1970).
30. Angert, E.R., Brooks, A.E. & Pace, N.R. Phylogenetic analysis of Metabacterium polyspora: clues to the evolutionary origin of daughter cell production in Epulopiscium species, the largest bacteria. *J Bacteriol* **178**, 1451-6 (1996).
31. Angert, E.R. & Losick, R.M. Propagation by sporulation in the guinea pig symbiont Metabacterium polyspora. *Proc Natl Acad Sci U S A* **95**, 10218-23 (1998).
32. Angert, E.R. & Clements, K.D. Initiation of intracellular offspring in Epulopiscium. *Mol Microbiol* **51**, 827-35 (2004).
33. Angert, E.R., Clements, K.D. & Pace, N.R. The largest bacterium. *Nature* **362**, 239-41 (1993).
34. Duda, V.I., Lebedinsky, A.V., Mushegjan, M.S. & Mitjushina, L.L. A new anaerobic bacterium, forming up to five endospores per cell —Anaerobacter polyendosporus gen. et spec. nov. *Archives of Microbiology* **148**, 121-127 (1987).
35. Chase, D.G. & Erlandsen, S.L. Evidence for a complex life cycle and endospore formation in the attached, filamentous, segmented bacterium from murine ileum. *J. Bacteriol.* **127**, 572-583 (1976).
36. Angert, E.R. Alternatives to binary fission in bacteria. *Nat Rev Microbiol* **3**, 214-24 (2005).
37. Cole, J.R. et al. The Ribosomal Database Project: improved alignments and new tools for rRNA analysis. *Nucl. Acids Res.* **37**, D141-145 (2009).

Movie 1. Partial penetrance of spoIIR^{PP} strains. Shown is a *spoIIR^{delay}* microcolony growing and sporulating (strain AES528). Cells are marked by a forespore specific σ^F reporter (green) and mother-cell specific σ^E reporter (red). Arrows indicate cells according to the following color code: Orange – sporulation, yellow – dispore, magenta – escape, green – twin. Individual frames are 20 min apart.

Movies 2. *C. oceanicum* sporulation – Shown are three channels of a time-lapse movie of a sporulating *C. oceanicum* colony; Phase contrast (left), DNA marker (Vybrant DyeCycle Green, middle) and membrane marker (FM4-64, right). Individual frames are 10 min apart. See Methods for more details on *C. oceanicum* time-lapse procedures.